Contribution to the knowledge of the relationship between the electrochemical and corrosion behaviour and the structure of metallic materials subjected to cold plastic deformation

By *B. Mazza, P. Pedeferri, D. Sinigaglia, U. Della Sala* and *L. Lazzari*

Istituto di Chimica Fisica, Elettrochimica e Metallurgia del Politecnico di Milano – Centro di Studio del C. N. R. sui processi elettrodici

Introduction

The present investigation forms part of a systematic study in the course of development at the Institute of Physical Chemistry, Electrochemistry and Metallurgy of Milan Polytechnic about the influence of cold plastic deformation on the electrochemical and corrosion behaviour of metallic materials with the aim of determining and elucidating such aspects of their behaviour and correlating them with "microstructural" effects of the deformation, these being analysed not only by metallographic and X-ray techniques but also by transmission electron microscopy.

From a general point of view there is an unanimous recognition that the thermodynamic-type influence exerted by cold plastic deformation (which can be ascribed to variations in the activity of atoms constituting the metallic material and therefore in the equilibrium electrode potential), is very little as compared with kinetic-type influence. Nevertheless, this result accompanied on the one hand by the difficulty of establishing in the various cases the significance of the potentials measured (true equilibrium potentials or corrosion potentials also determined by kinetic factors) and, on the other hand, by the poor comparability of the working conditions, makes the variation in the equilibrium potentials due to work-hardening difficult and uncertain in its determination not only as regards its value but even its sign.

The interpretation, if not in fact the existence, of the influence of a state of deformation following a process of cold working are also controversial so far as concerns the kinetic aspects of the electrochemical and corrosion behaviour of ferrous materials in the active region.

In general, with increasing degree of work-hardening the rate of generalized corrosion under conditions of active material increases, even though, as can be seen in Table 1, there are also cases in which no effect of cold plastic deformation is observed*) (1). Such discrepancies of the results may still be ascribed to poor comparability of the working conditions, especially as regards the type and the degree of the deformation and the qualitative and also quantitative composition of the aggressive medium, apart from considering the intrinsic lack of reproducibility in the behaviour of ferrous materials used technically owing to the effect of uncontrollable factors such as impurities or surface films.

Analysing corrosion resistance into its components, some authors (*Evans, Greene* (1), *Hoar* et al. (2)) attribute the observed increase in the corrosion rate with increasing degree of work-hardening of the material to a decrease in the anodic overvoltage due to a greater number of surface centres with low activation energy for anodic dissolution (emerging dislocations, pile-ups of dislocations and stacking faults), while other authors (*Foroulis, Uhlig, Trabanelli* (1)) are of the opinion that the acceleration of the corrosive phenomena induced by cold plastic deformation is due only to a decrease in cathodic overvoltage for hydrogen evolution in consequence of an increase in the number of active centres that catalyze it (such as impurity atoms, for example carbon, concentrated in correspondence with the dislocations, to form *Cottrell* atmospheres).

*) Obviously, in the absence of circumstances that could mask the influence of the deformation, as for example when the corrosion rate is controlled by the supply of dissolved oxygen by diffusion.

Table 1. Effect of cold plastic deformation on corrosion rate of metallic materials

Investigator (Ref. (1))	Metallic material	Deformation type	Environment (deaerated solution)	Corrosion rate
Tammann and *Neubert*	Electrolytic iron	Cold-rolling	Sulphuric acid	Increased
Heyn and *Bauer*	Carbon steel	Cold-drawing	Sulphuric acid	Increased
Edwards, Phillips and *Thomas*	Mild steel	Cold-rolling	Sulphuric acid; citric acid	Slightly increased
Simnad and *Evans*	Pure iron; mild steel	Cold-rolling	Hydrocloric acid	Increased
Greene and *Saltzman*	Zone-refined iron	Torsion	Sulphuric acid; hydrocloric acid	Increased
	Carbon steels	Torsion; cold-rolling	Sulphuric acid; hydrocloric acid	Increased
Foroulis and *Uhlig*	Zone-refined iron	Cold-rolling	Hydrocloric acid	Unaffected
	Mild steel	Cold-rolling	Hydrocloric acid	Increased
Foroulis	Iron-carbon-silicon alloys	Cold-rolling	Hydrocloric acid	Increased
Zucchi, Zucchini, Trabanelli and *Baldi*	ARMCO iron	Cold-rolling	Hydrocloric acid	Increased
France	Rimmed steel	Torsion	Ammonium nitrate	Increased
Franks	AISI 304, 316 and 347 austenitic stainless steels	Cold-rolling	Nitric acid	Unaffected
Copson	Nickel	Unspecified cold-working	Hydrocloric acid; sodium hydroxide	Unaffected
Trabanelli and *Zucchi*	Nickel	Cold-rolling	Sulphuric acid	Unaffected

In general, the possibility that the work-hardening process enhances the causes of heterogeneity of the metallic material (for example, through the precipitation of new phases, phase transformations, segregation of impurities, formation of substructures, preferred orientation of the crystal grains, local variation in the surface chemical composition due to appearance of segregates on the surface, etc.) with striking consequences on the corrosion rate is also assumed (1, 3).

The considerations mentioned above relate to ferrous materials with film-free surfaces. Otherwise one must obviously take into account (and this is then probably the dominant influence on the corrosion rate) the degradation caused by cold plastic deformation in the protective characteristics of the passivating films owing to the formation of fissures, cracks, etc. (3).

The present study of the influence of cold plastic deformation on the electrochemical and corrosion behaviour of metallic materials relates above all to some of the principal austenitic stainless steels in common use, because of the absence of information available in the literature on such materials and also in view of the possibility of drawing conclusions of applicative nature from the consideration of peculiar aspects of their corrosion behaviour, such as their susceptibility to pitting and to stress corrosion. In this spirit the deformation process examined initially was cold drawing (4).

The necessity to specify in the best possible way the working conditions in order to avoid the scatter and even the contradictory nature of the results found in the literature for other materials, with consequent uncertainties of interpretation, forces us (supported in this respect by some preliminary results) to consider as another possible factor of influence of cold plastic deformation the orientation of the exposed surface with respect to the deformation direction. According to this idea and also in view of the correlation it was intended to establish with the microstructural effects produced by cold plastic deformation, the deformation by the application of a tensile stress presented the following advantages as compared with other types of deformation more significant from a practical point of view, such as cold-drawing, rolling, or pressing:

a) The advantage of leading in the course of the deformation process to a better-defined situation so far as concerns the distribution of stresses within the test-piece;
b) Consequently the advantage of relating the work to be carried out to three significant orientations of the exposed surface, namely, besides those perpendicular and parallel to the axis of tension, that oriented at 45 ° with respect to it[x]), because of the predictable corresponding marked effect of shear stress;
c) Finally the advantage of leading to a better-defined and simpler situation from a microstructural point of view as well, since it is possible to a first approximation to consider as negligible, in comparison with the other effects induced by cold plastic deformation, the effect of preferred orientation of the crystal grains (5) (a situation confirmed by X-ray and metallographic analyses).

As regards the materials examined, in order to permit a more complete phenomenological picture to be obtained, and also with a view to achieving better interpretations, the investigation was extended to two of the principal components of austenitic stainless steels (easily susceptible to deformation), namely iron and nickel.

The electrochemical and corrosion behaviour of the metallic materials considered in de-aerated sulphuric acid solution was recorded both in overall terms of corrosion potential and rate of generalized corrosion under conditions of active material, determined by *Stern* and *Geary's* electrochemical method (6), and in analytical terms of partial anodic and cathodic processes, by determining the relative characteristic curves extended, on the anodic side, to consider the passive region as well.

Finally, observations were made with the aid of transmission electron microscopy on deformed materials, in order to determine the nature, the distribution, and the density of structural defects present, and the various possible phases differing from the matrix induced by the deformation.

Experimental Part

I. Materials investigated

The chemical compositions of the metallic materials studied are given in Table 2.

Such materials, initially in the form of hot-rolled rods with a diameter of 25–35 mm, were subjected to the following operations:

1a) For the austenitic stainless steels: solubilization of any carbides present by heating to 1050 °C for about 20 min. with subsequent cooling in water;
1b) For the iron: annealing at 760 °C with cooling in air;
1c) For the nickel: annealing at about 850 °C with cooling in air *);
2. Deformation by the application of a tensile stress **) until the following reductions in the cross-sectional area of the test-pieces had been achieved ***):
2a) 5, 15, and 30% for the austenitic stainless steels;
2b) 5, 10, and 15% for the iron;
2c) Also 5, 15, and 30% for the nickel;
3. Cutting, working on the lathe, and preliminary polishing with dry papers to obtain the test specimens;

[x]) Subsequently for the sake of brevity we shall use the following abbreviations for the surface orientations: T for transverse, L for longitudinal, and 45 ° I for the 45 ° inclined orientation.

*) Operations 1a-c were performed at the works.
**) So that the length of the standardized tensile test-pieces (UNI 551-69) used increased at a constant rate of ~ 0.5 mm/sec. Only the central part of such test-pieces was used.
***) Values adopted to express the degree of work-hardening of the material.

Table 2. Chemical composition of metallic materials studied

Metallic material	Weight % composition										
	Fe	C	Mn	Si	Cr	Ni	Mo	Cu	S	P	Other
AISI 304	bal.	0.055	1.45	0.68	18.70	8.91	0.146	0.094	0.014	0.036	–
AISI 304 L	bal.	0.025	1.44	0.47	19.11	9.64	–	–	0.014	0.023	–
AISI 316	bal.	0.045	1.44	0.76	16.90	11.25	2.50	–	0.012	0.040	–
ARMCO Iron	bal.	0.017	–	–	–	–	–	0.03	0.005	0.012	–
Nickel L	0.06	0.023	0.26	<0.05	–	bal.	–	<0.03	0.005	–	Co 0.044

4. Surface preparation of the samples by polishing with wet papers with decreasing grain size (70, 35, 25 and 15 μ); electrolytic polishing in a solution of ethanol and perchloric acid followed again by wet polishing with 15 μ papers; polishing with diamond pastes (7, 3 and 1 μ) and finally mixed mechanical and electrolytic polishing (Relapol).

II. Electrochemical Measurements

All the electrochemical measurements were made with the aid of a cell developed by the present authors (4), which is shown in vertical section in Fig. 1 and which has the following main characteristics:

1. Solution volume ~ 500 ml, with the ratio of the solution volume (cm^3) to the exposed area of the sample (cm^2) ~ 500;
2. Electrode-holder consisting of three parts (made of insulating material) screwing into one another, which permits precise delimitation of the exposed area of the sample without phenomena of localized crevice corrosion and, also complete and rigorous insulation of the electrical contacts from the solution.
3. A distance between the end of the capillary probe of the *Luggin-Haber* type connected to the reference electrode and the electrode surface of 1–2 mm (adjustable by means of a ball joint), which enables the error due to the ohmic drop and to the shielding effect in the measurement of the overvoltages to be minimized;
4. Separation of the electrode compartment from the remaining volume of the solution by means of a porous diaphragm which ensures the absence of interference with the electrode processes under study due to a possible evolution of oxygen at the counterelectrode.

A 1M solution of H_2SO_4 (Carlo Erba RP reagent), deaerated and stirred by circulation of H_2 gas, at a temperature of 25 °C, was used for all the measurements.

As already stated, the generalized corrosion rate of the various materials in the active region was determined by the method of *Stern* and *Geary**) consisting in the recording of

*) Apart from measurements of the loss of weight in some cases for checking purposes.

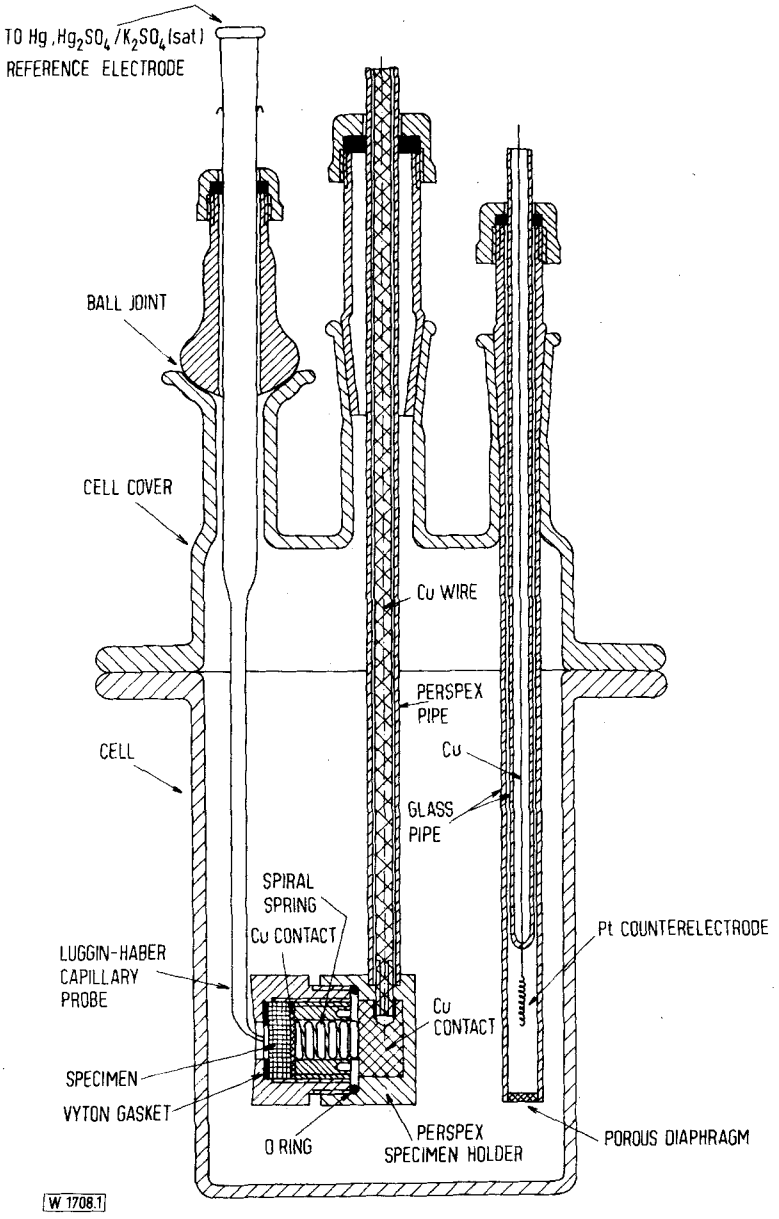

Fig. 1. Test cell (vertical section)

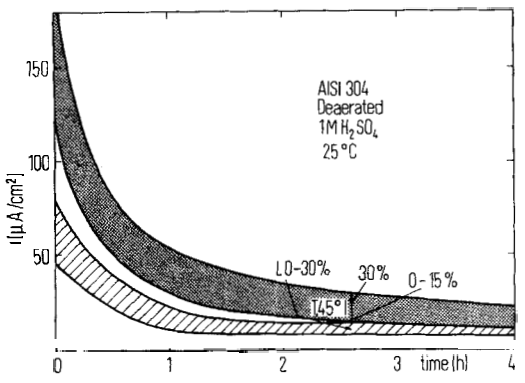

Fig. 2. Corrosion rates of AISI type 304 steel in deaerated 1M H_2SO_4 solution at 25 °C as a function of time, deformation degree (indicated per cent and obtained by application of a tensile stress) and orientation of the exposed surface to the deformation direction (L, T and 45 °I correspond to surfaces which are respectively parallel, perpendicular and inclined at 45 ° to the deformation direction). i-values on the ordinate axis are the external current densities recorded in the *Stern-Geary* technique

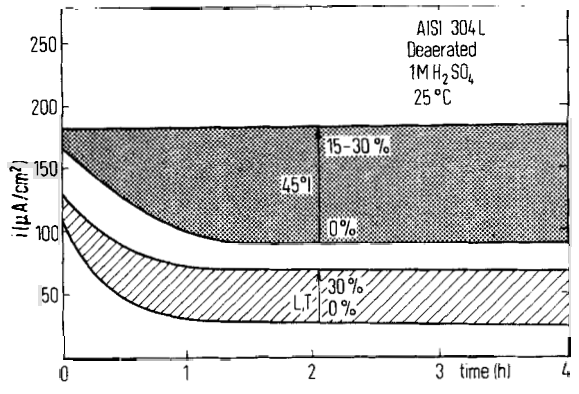

Fig. 3. Corrosion rates of AISI type 304 L steel in deaerated 1M H_2SO_4 solution at 25 °C as a function of time, deformation degree and orientation of the exposed surface

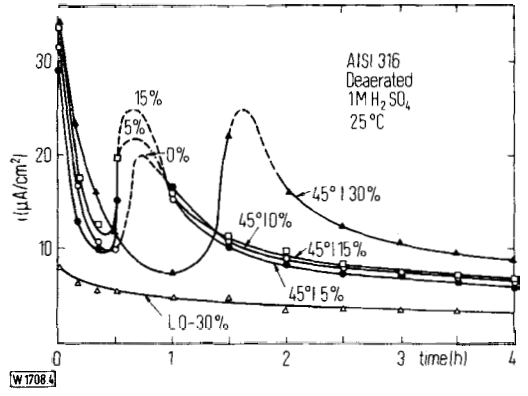

Fig. 4. Corrosion rates of AISI type 316 steel in deaerated 1M H_2SO_4 solution at 25 °C as a function of time, deformation degree and orientation of the exposed surface.
T surfaces show the same behaviour as 45 °I surfaces

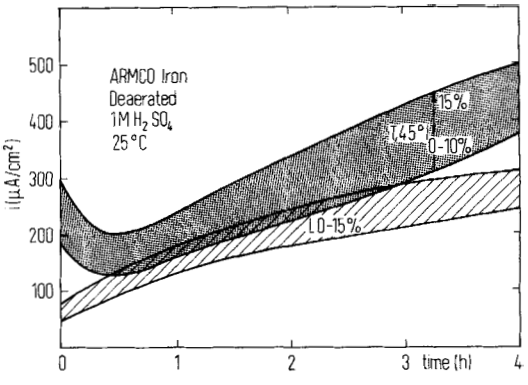

Fig. 5. Corrosion rates of ARMCO iron in deaerated 1M H_2SO_4 solution at 25 °C as a function of time, deformation degree and orientation of the exposed surface

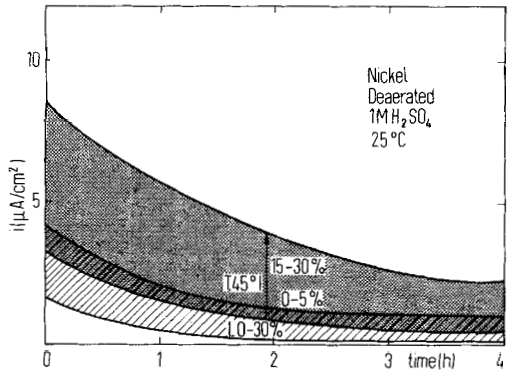

Fig. 6. Corrosion rates of nickel in deaerated 1M H_2SO_4 solution at 25 °C as a function of time, deformation degree and orientation of the exposed surface

the circulating current (shown directly in the graphs of Figs. 2–6 and, as is well known, proportional to the corrosion rate) after the application to the sample of a rectangular voltage pulse in the cathodic or anodic direction with an amplitude sufficiently small to remain within the range of linearity of the voltage-current characteristic. The currents due to the application of rectangular voltage pulses in the cathodic direction, with an amplitude of 10 mV and a duration of 1 min, were measured during the first 4 h every 1/2 h (and in the first 1/2 h every 10 min).

At the end of each test (i. e. after 4 h) the curves of cathodic overvoltage relative to the evolution of hydrogen were recorded. The long immersion time guaranteed that more reproducible results were obtained*) (7).

*) In particular, the polarization curves recorded immediately after immersion of the sample in the solution showed no definite effect of the degree of work-hardening, owing to the prevalence of irreproducible effects due to variations in surface chemical composition. Moreover, in spite of the increase in the effective electrode surface in relation to the apparent surface, especially in the case of the more easily corroded materials (iron and AISI 304 L steel), the errors in the current density values due to such long preliminary time of contact of the electrode with the solution do not change the essence of the results obtained.

The cathodic overvoltage curves were recorded in triplicate by three variants of the potentiostatic method:

1. Stepwise increase, in the cathodic direction, of the potential of the electrode under measurement relative to the reference electrode by an amount of 10 mV every 15 sec;
2. Application to the sample of rectangular voltage pulses in the cathodic direction, lasting 15 sec and at intervals of 1 min, with an amplitude increasing by 10 mV each time, always in relation to the initial value of the corrosion potential;
3. Application to the sample of rectangular voltage pulses in the cathodic direction, lasting 15 sec and at intervals of 1 min, with an amplitude increasing each time by 10 mV with respect to the actual value of the corrosion potential.

These three methods led to practically coincident results (fig. 12).

The anodic polarization curves were recorded by the potentiodynamic method, with a scanning rate of the electrode potential of 20 mV/min. In the case of iron the anodic characteristics in the active region were also determined potentiostatically by the method 2 described above for the cathodic characteristics (the amplitude of the voltage pulses was increased by 20 mV each time; the pulse lasted 5 sec and the interval between two successive pulses was 1 min).

An AMEL Model 551/SU apparatus was used for all the electrochemical measurements.

The electrode potentials were always referred to the Hg, Hg_2SO_4/K_2SO_4 (sat.) electrode (=SSE), the potential of which relative to the standard hydrogen electrode at 25 °C is + 642 mV*).

III. Microstructural Investigations

The electron-microscope investigation was performed for all the materials in the two states of "as received" (i. e. after operations 1a, 1b, or 1c as listed earlier, p. 240) and of maximum deformation, on the surface perpendicular to the axis of tension. For steel AISI 304 L the intermediate values of the deformation degree and the surface orientations parallel to and inclined at 45° to the axis of tension were also considered.

The samples for observation under the electron microscope were in the form of discs 3 mm in diameter, obtained by punching from sheets cut with the desired orientation with respect to the deformation direction and polished to a thickness of 200–300 μ. These discs were then thinned down electrolytically in a Struers Tenupol apparatus, which controls the final thickness of the central part of the disc automatically by means of a source of light and a photocell. The transparent zones of the sample, with a thickness of the order of 1000–2000 Å, were examined in the Philips EM 300 electron microscope to 100 kV**).

Results

I. Electrochemical Measurements

The results concerning the electrochemical and corrosion behaviour of the metallic materials investigated are illustrated in Figs. 2–19, and can be summarized as follows.

With increasing deformation degree there was (Figs. 2–6) an increase in the generalized corrosion rate in the active region on the exposed surfaces of the samples oriented perpendicularly or at 45° to the axis of tension, while on the surfaces oriented parallel to this axis, except for the case of the steel AISI 304 L, no definite tendency was found for a change in the corrosion rate with increasing deformation degree, the variation measured being within the range of scatter of the experimental results. Furthermore, again with the exception of AISI 304 L, on the surfaces considered last (L surfaces) the corrosion rate was lower, for equal degree of work-hardening, than on the former (T and 45° I surfaces).

Taking into account the intrinsic lack of reproducibility in the behaviour of the materials investigated, the described effects of the degree of work-hardening and of the orientation of the exposed surface with respect to the deformation direction on the corrosion rate are rather weak from the quantitative point of view (the maximum variations of the corrosion rate being within a factor of 2–4), although when such effects can be detected they indicate a definite tendency (confirmed, moreover, by weight loss measurements performed for control purposes). Such considerations are particularly valid for the materials with the lowest corrosion rates : AISI 316 and nickel.

Again from a quantitative point of view, the influence of the degree of work-hardening is shown to an appreciable extent above a critical threshold which in our case we can place roughly (given the discrete series of degrees of work-hardening that we considered) at about 10% for iron and nickel and at 15% for the austenitic stainless steels. Among the latter, the susceptibility to the effect of cold plastic deformation increases in the sequence :

AISI 316 < AISI 304 < AISI 304 L.

Steel AISI 304 L is still more sensitive to the effect of variations in the degree of work-hardening with regard to the corrosion rate when it is deformed by cold drawing rather than by the application of a tensile stress (4).

Considering the anisotropy of the behaviour of surfaces with different orientations in relation to the axis of tension, it may be observed that this is manifested even for zero work-hardening, i. e. in a material not deformed by tension. This can obviously be explained only by an influence of the operations undergone by the test-pieces independently of deformation by tension, an influence that is not cancelled out by the solubilization or annealing treatments described above (p. 240).

Finally, so far as concerns the time-dependence of the corrosion rates, these increase with time in the case of iron×), but decrease to reach steady values after 4 h in the case of the AISI 304 and 304 L steels and in the case of nickel, while the corresponding corrosion potentials remain practically constant within the limits of reproducibility of the measurements (20–30 mV××)). In the case of steel AISI 316 (fig. 4), on the T and 45° I surfaces, after a rapid initial decrease the corrosion rate begins to increase again, then to decrease once more, finally reaching a steady value. Correspondingly, the corrosion potential of AISI 316 becomes more noble to an extent of ~ 100 mV in the course of 4 h (Fig. 7). The time

*) The contribution of the liquid junction potential was minimized by connecting the reference electrode through an agar-agar bridge with a saturated solution of KNO_3.

**) For the performance of the electron microscope observations we are indebted to Dr. *D. Wenger* of CISE, Segrate.

×) In this case, however, a non-negligible increase occurred in the effective surface of the samples during the measurement, in relation to the initial apparent surface used for the calculation of the current densities shown in Figs. 2–6.

××) This erratic nature of the corrosion potentials is sufficient to mask the effects of the deformation degree and of the orientation (L, T, 45°I) of the electrode surface.

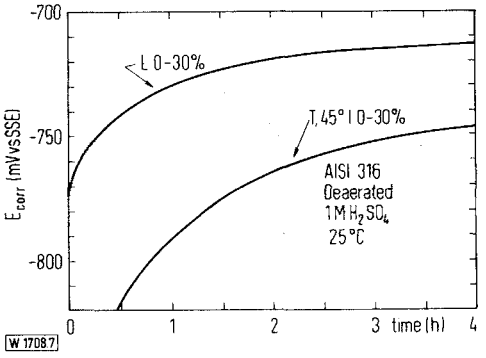

Fig. 7. Average values of corrosion potentials (relative to a saturated mercury sulphate electrode, SSE) of AISI type 316 steel in deaerated 1M H_2SO_4 solution at 25 °C as a function of time, deformation degree and orientation of the exposed surface

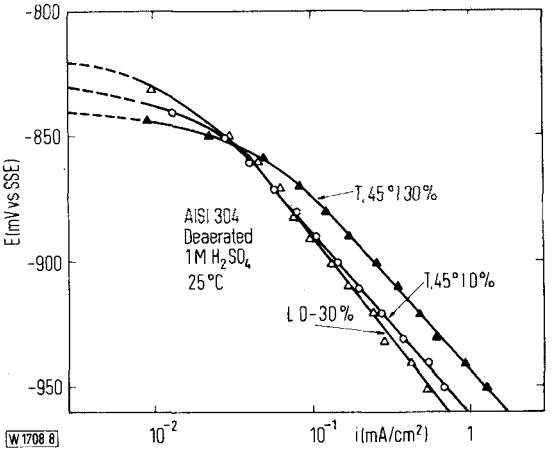

Fig. 8. Cathodic polarization curves for hydrogen evolution on AISI type 304 steel in deaerated 1M H_2SO_4 solution at 25 °C for different degrees of deformation and orientations of the electrode surface

corresponding to the minimum and the maximum of the corrosion rate curve increases when the material is strongly work-hardened. On the L surface, on the other hand, the corrosion rate decreases monotonically with time, as for the other steels, always remaining lower than on the T and 45 °I surfaces; the corresponding increase in the corrosion potential (which already starts from higher values) is ~ 50 mV in 4 h.

Analysis of the corrosion behaviour in terms of partial anodic and cathodic processes has shown that, for all the materials investigated, a decrease (within maximum limits of some 20–40 mV) in the overvoltage of the cathodic hydrogen evolution*) always corresponds to an increase in the corrosion rate when the deformation degree or the orientation of the exposed surface are varied, and conversely, when the influence of the above-mentioned factors on the corrosion rate cannot be definitely established, the effect on the hydrogen overvoltage cannot be detected either (Figs. 8–13).

The decrease in the hydrogen overvoltage with increasing degree of work-hardening is shown by a displacement of *Tafel's* straight lines parallel to one another in the direction of higher current densities, while the relative slopes remaining unchanged**).

In conclusion, even in the case of cold plastic deformation obtained by tension (besides that obtained by drawing (4)), and with the materials and the conditions under which we operated, it has been possible to establish the existence of an anticorrelation between the results relating to the influence of the degree of work-hardening and of the orientation of the exposed surface with respect to the deformation direction, on the hydrogen overvoltage on the one hand and on the corrosion rate on the other hand; as a matter of fact, this influence corresponds to changes in the two properties (hydrogen overvoltage and corrosion rate) that are of opposite sign and of magnitude mutually correlatable in biunivocal fashion.

On the other hand, the anodic behaviour of the materials considered in the active region (Figs. 14–19) is not appreciably affected by the degree of work-hardening***), with the exception of the case of iron, for which, with increasing degree

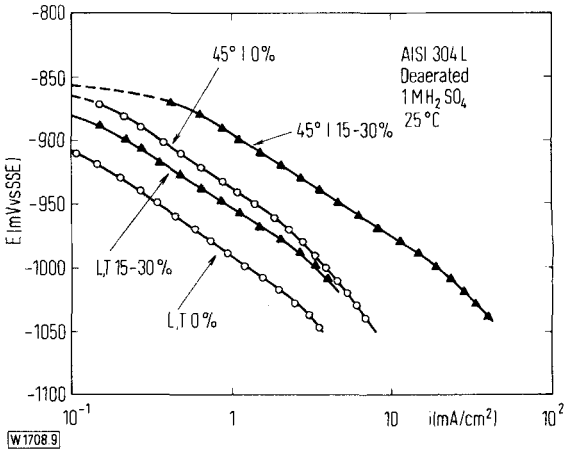

Fig. 9. Cathodic polarization curves for hydrogen evolution on AISI type 304 L steel in deaerated 1M H_2SO_4 solution at 25 °C for different degrees of deformation and orientations of the electrode surface

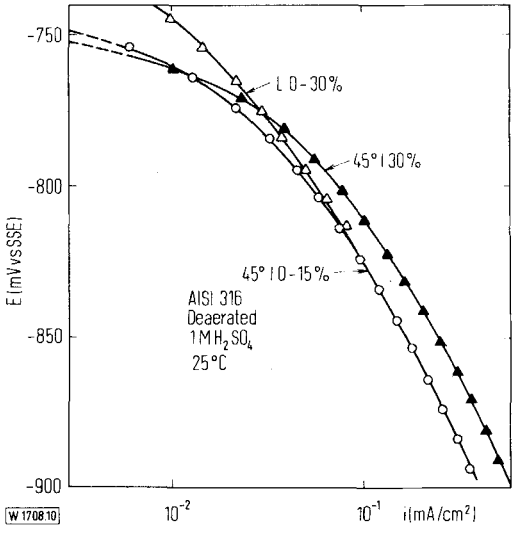

Fig. 10. Cathodic polarization curves for hydrogen evolution on AISI type 316 steel in deaerated 1M H_2SO_4 solution at 25 °C for different degrees of deformation and orientations of the electrode surface

*) Also in the case of titanium deformed by application of a tensile stress equal to 90% of the yield strength the hydrogen overvoltage in boiling 0.1 M H_2SO_4 diminishes in comparison with the undeformed material (private communication of *G. Taccani* and *B. Vicentini*, Laboratorio Tecnologia Materiali non Tradizionali del C. N. R., Cinisello Balsamo).

**) With values between 80 and 100 mV for the various materials considered.

***) For the austenitic stainless steels studied the slopes of the anodic *Tafel* lines are of the order of 40 mV.

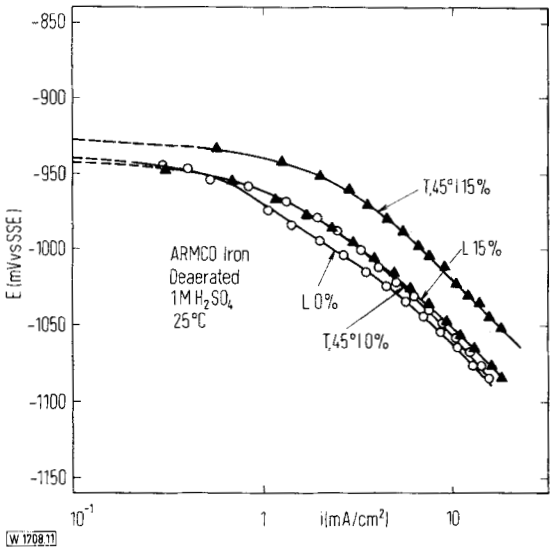

Fig. 11. Cathodic polarization curves for hydrogen evolution on ARMCO iron in deaerated 1M H_2SO_4 solution at 25 °C for different degrees of deformation and orientations of the electrode surface

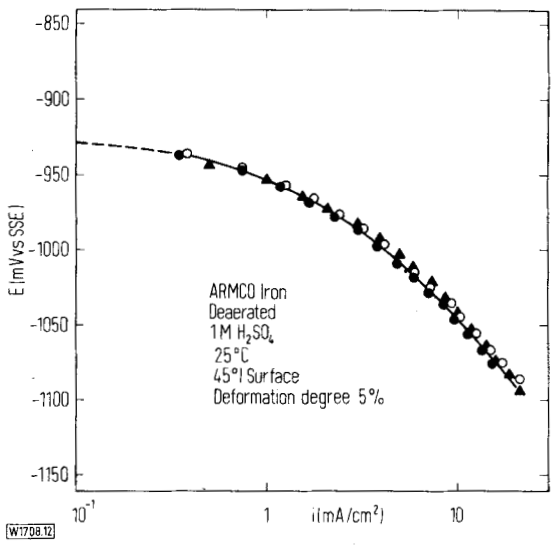

Fig. 12. Cathodic polarization curves for hydrogen evolution on ARMCO iron in deaerated 1 M H_2SO_4 solution at 25 °C, plotted with the three methods described in the text (p. 243): ● method 1; ○ method 2; ▲ method 3.

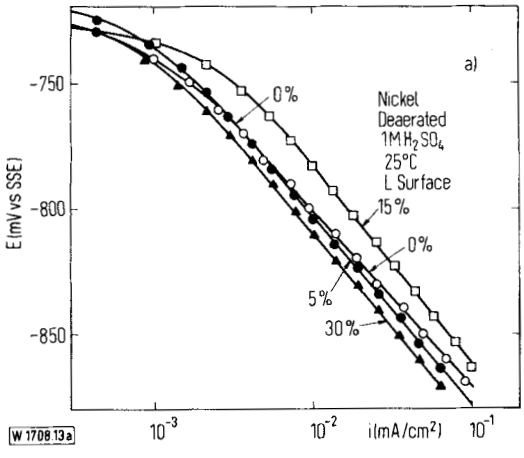

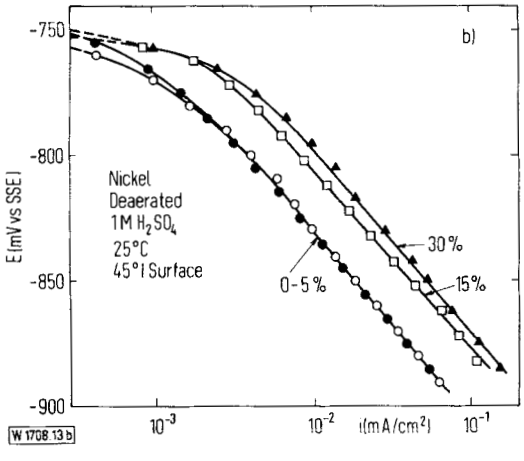

Fig. 13. Cathodic polarization curves for hydrogen evolution on nickel in deaerated 1M H_2SO_4 solution at 25 °C for different degrees of deformation and orientations of the electrode surface (a and b)

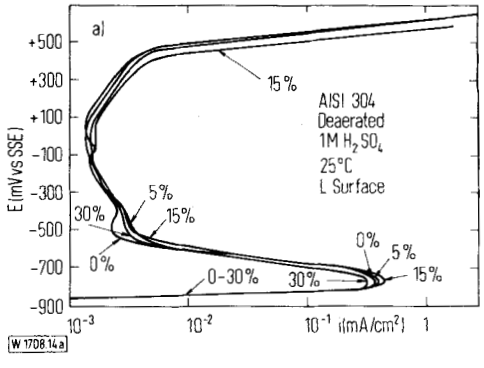

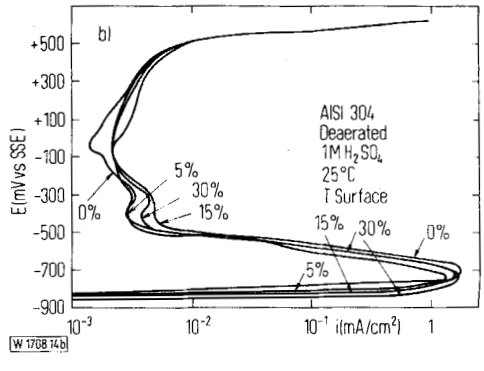

Fig. 14. Potentiodynamic anodic polarization curves of AISI type 304 steel in deaerated 1M H_2SO_4 solution at 25 °C for different degrees of deformation and two orientations (a and b) of the electrode surface

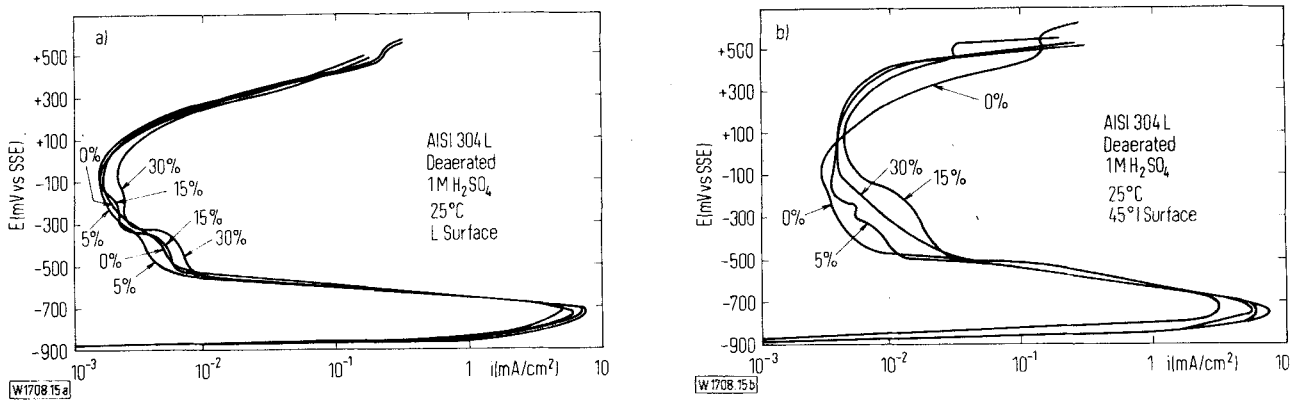

Fig. 15. Potentiodynamic anodic polarization curves of AISI type 304 L steel in deaerated 1 M H_2SO_4 solution at 25 °C for different degrees of deformation and two orientations (a and b) of the electrode surface

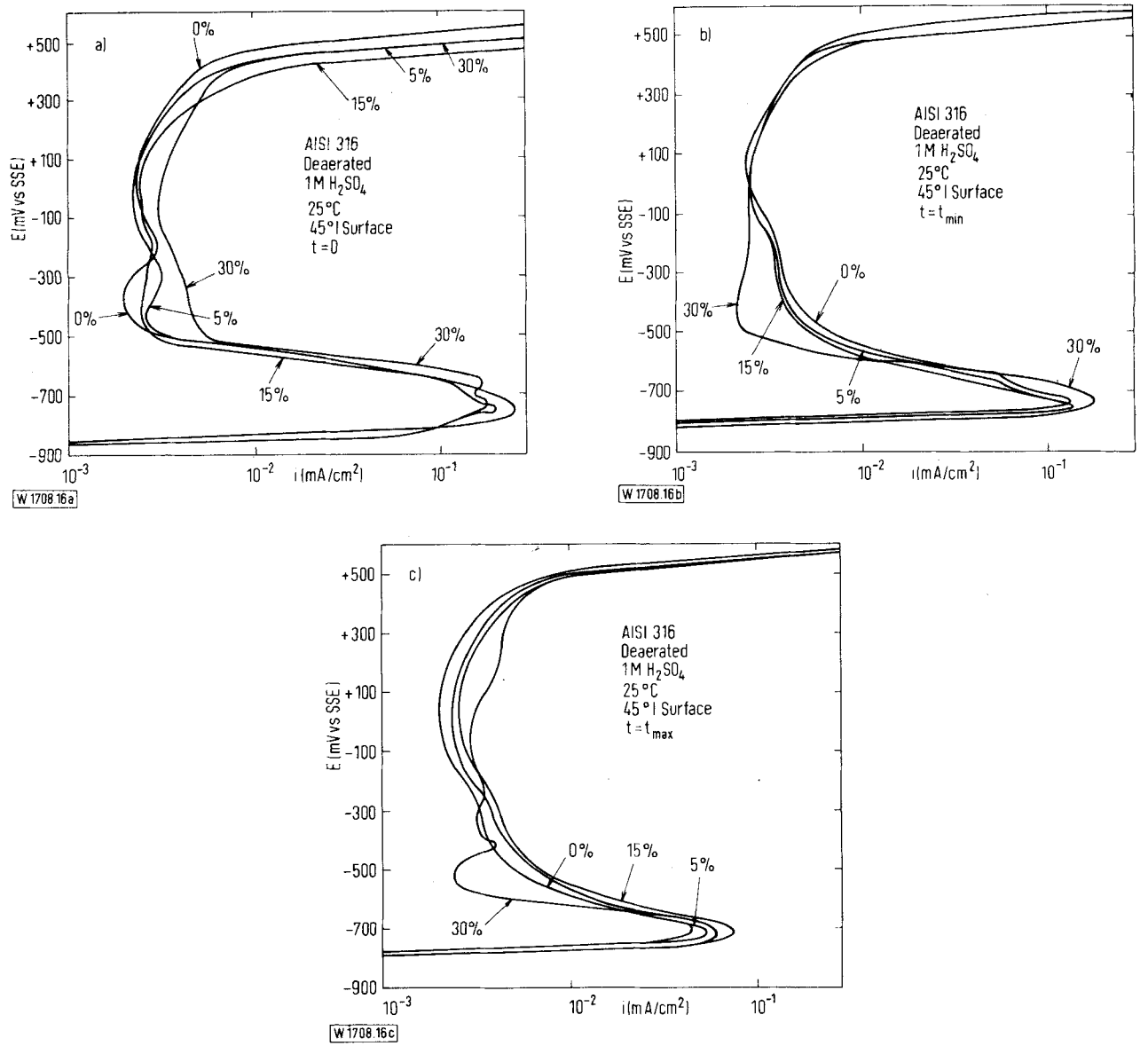

Fig. 16. Potentiodynamic anodic polarization curves of AISI type 316 steel in deaerated 1 M H_2SO_4 solution at 25 °C for different degrees of deformation and three typical immersion times (a, b and c, which correspond to : t = 0, t = t_{min} and t = t_{max} of fig. 4)

of work-hardening, besides a decrease in the cathodic overvoltage, a decrease in the anodic overvoltage is also found.

Extending the investigation beyond the active range, the greater work-hardening of the material in the case of the austenitic stainless steels was accompanied by a well-defined negative effect which is shown in the active to passive transition region of the anodic polarization curve in a retarded formation of the passivating films (Figs. 14–16). No precise relationship appears to exist in the passive region between the degree of work-hardening and the stability and the protective characteristics of the passivating films. A more stable passivity is generally shown on the L surface than on the T and 45 °I surfaces (Figs. 14 and 15).

The case of AISI 316 deserves some additional consideration relative to the anomalous shape of the corrosion curve as a function of time on the T and 45 °I surfaces (Fig. 4). In this case the anodic characteristic was recorded not only immediately after immersion of the samples in the solution (t = O), but also at times of the minimum ($t = t_{min}$) and the maximum ($t = t_{max}$) of the corrosion curve. It is evident from Fig. 16 that the behaviour of AISI 316 changes in the period between t = O and $t = t_{min}$ and subsequently $t = t_{max}$, in the sense of gradually assuming a greater practical nobility and a greater passivability.

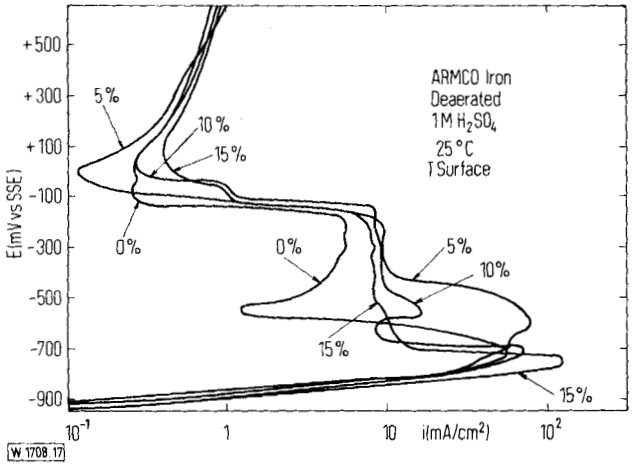

Fig. 17. Potentiodynamic anodic polarization curves of ARMCO iron (horizontal, upwards-facing anodes) in deaerated 1 M H_2SO_4 solution at 25 °C for different values of the deformation degree

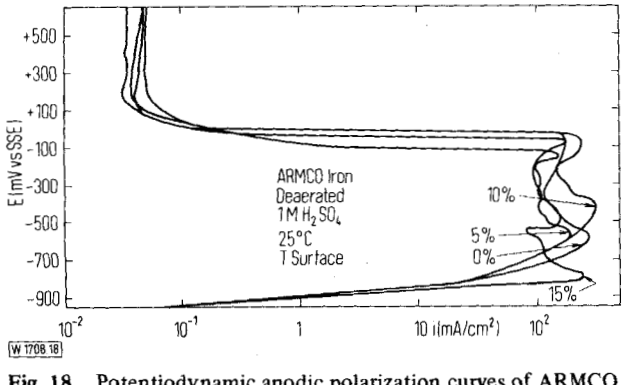

Fig. 18. Potentiodynamic anodic polarization curves of ARMCO iron (vertical anodes) in deaerated 1 M H_2SO_4 solution at 25 °C for different values of the deformation degree

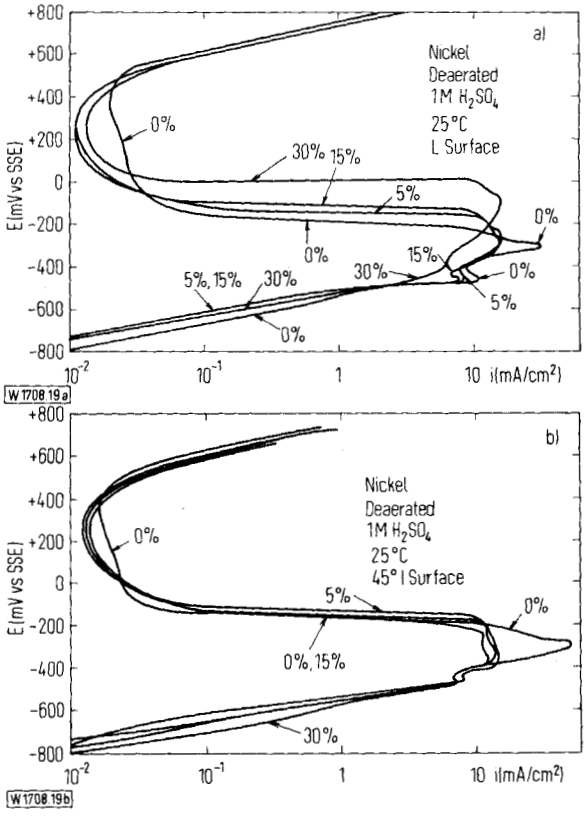

Fig. 19. Potentiodynamic anodic polarization curves of nickel in deaerated 1 M H_2SO_4 solution at 25 °C for different degrees of deformation and two orientations (a and b) of the electrode surface

In the case of iron, the shape of the anodic polarization curves beyond the active range is strongly affected by the surface position (horizontal facing upwards (Fig. 17) or vertical (Fig. 18)) of the electrode, while it does not depend significantly either on the degree of work-hardening or on the orientation (L, T, 45 °I) of the electrode surface with respect to the axis of tension.

Also in the case of nickel the formation of protective films is hindered by the work-hardening of the material, particularly on the L surfaces (Fig. 19). Moreover "as received" nickel shows higher values of the principal peak current and of the passive current than cold-deformed nickel, besides a more narrow active-passive loop and a more marked pseudo-passivation peak.

Both for the iron (in the two surface positions considered) and for the nickel the protective action of passivating layers is rather poor, being the passive currents at least 10 times higher than for the austenitic stainless steels: (10^{-2} – 10^{-1}) m A/cm² instead of (10^{-3} – 10^{-2}) m A/cm².

II. Microstructural Investigations

Comparative electron microscope examination of the various materials investigated has revealed the following points.

For the "as received" state, randomly-distributed dislocations are observed on all the materials (with densities of the order of 10^8/cm²), sometimes piled up at the grain boundaries (especially in the case of the AISI 316, Fig. 20a) or even concentrated around inclusions (which are often found at the grain boundaries), or, in the case of the AISI 304 L, around the ferrite present in small amounts. In particular, the nickel showed, even for a zero degree of deformation,

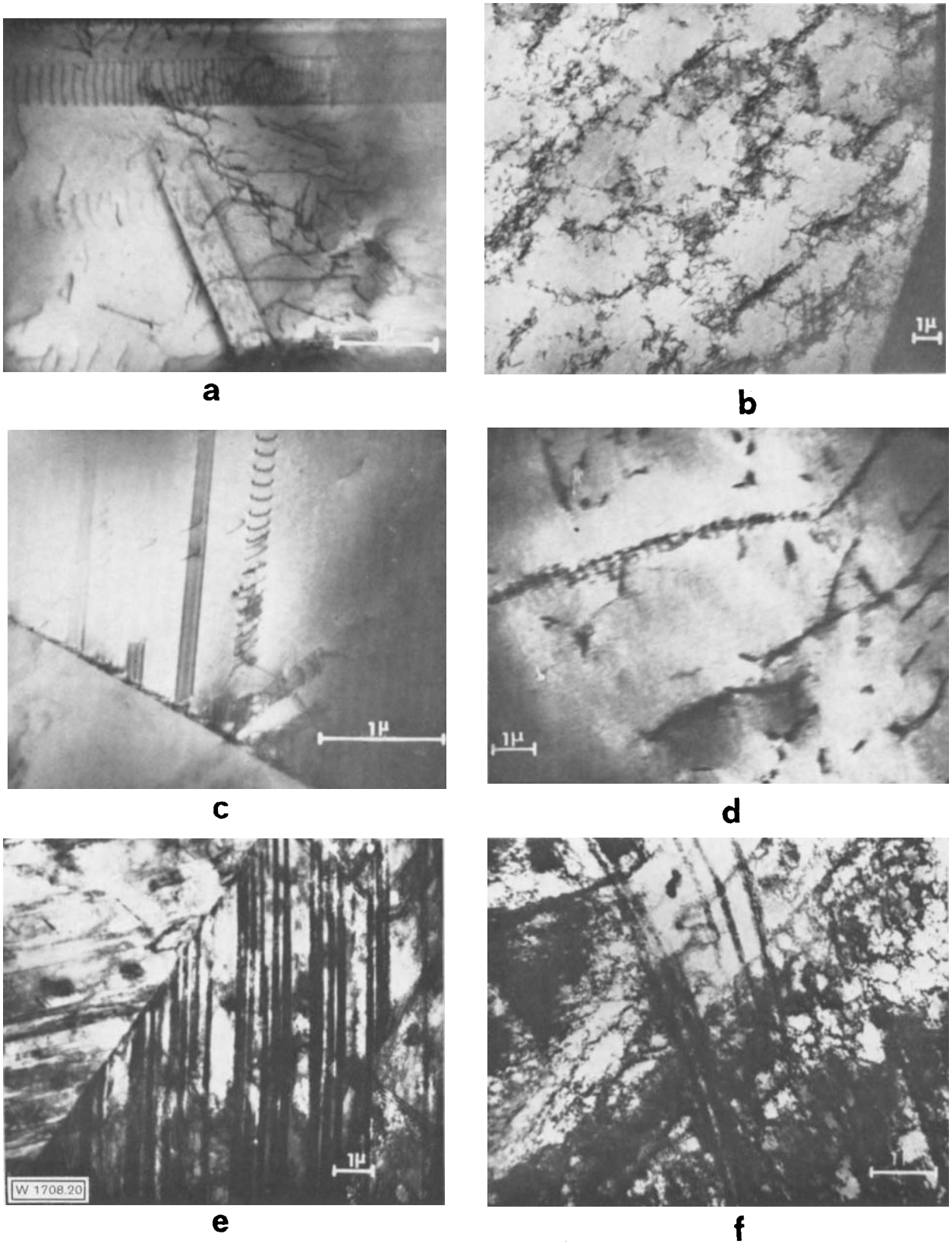

Fig. 20. Transmission electron micrographs (TEM) of different metallic materials undeformed or deformed by application of a tensile stress:

a) pile-up of dislocations at grain boundary on AISI type 316 steel in the "as received" condition;
b) dislocations arranged in a "cell structure" on nickel in the "as received" condition;
c) stacking faults and pile-ups of dislocations on AISI type 304 steel in the "as received" condition;
d) "decorated" dislocations on ARMCO iron in the "as received" condition;
e) deformation bands on AISI type 304 steel deformed 30 per cent;
f) deformation bands, "cellular" dislocations and tangled forests of dislocations on AISI type 304 L steel deformed 30 per cent.
a) . . . e): T surfaces; f): L surface

a tendency for the dislocations to be arranged in a cell structure*) (Fig. 20b), tendency to which the absence of pile-ups of dislocations corresponds. Stacking faults are present in steel AISI 304 (Fig. 20c) and, to a smaller extent, in the AISI 304 L, while they have not been observed in AISI 316, in nickel and in iron. In the iron the dislocations appear decorated, owing to the presence of precipitates or interstitial atoms anchored there (Fig. 20d).

On materials work-hardened to the maximum extent and examined on surfaces perpendicular to the deformation direction both the appearance of new types of structural defects and their increase in density is found. On the austenitic stainless steels deformation bands parallel to the slip planes are observed (Fig. 20e) in density decreasing on passing from AISI 304 to 304 L and 316. While on the AISI 304 the band structure is the only one that could be observed, on the 304 L and the 316 it is possible to detect the presence of a cell structure superimposed on the band structure, besides tangled forests of dislocations (Fig. 20f). In the case of the AISI 304 L it has been possible to establish by means of electron diffraction that the deformation bands can be resolved either as deformation twins (Fig. 21) or as α' cubic martensite (Fig. 22) produced by the phase transformation of austenite to martensite in consequence of the deformation**). On work-hardened nickel only the cell structure is observed (Fig. 23), no deformation bands appearing; again by electron diffraction it has been possible to show the disorientation that exists among the cells within a single grain. In the case of work-hardened iron the electron microscope examination has not yet given significant results because of the perturbation induced by the strong magnetic field set up by the sample in the magnetic field of the microscope objective.

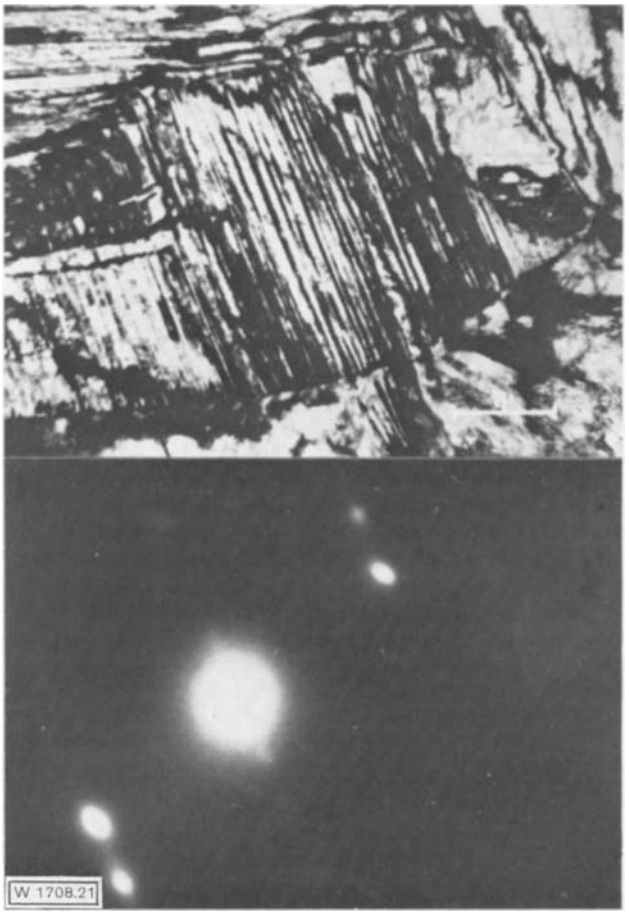

Fig. 21. TEM and selected-area electron diffraction pattern showing the identification of deformation twins in some deformation bands on AISI type 304 L steel deformed 30 per cent. L surface

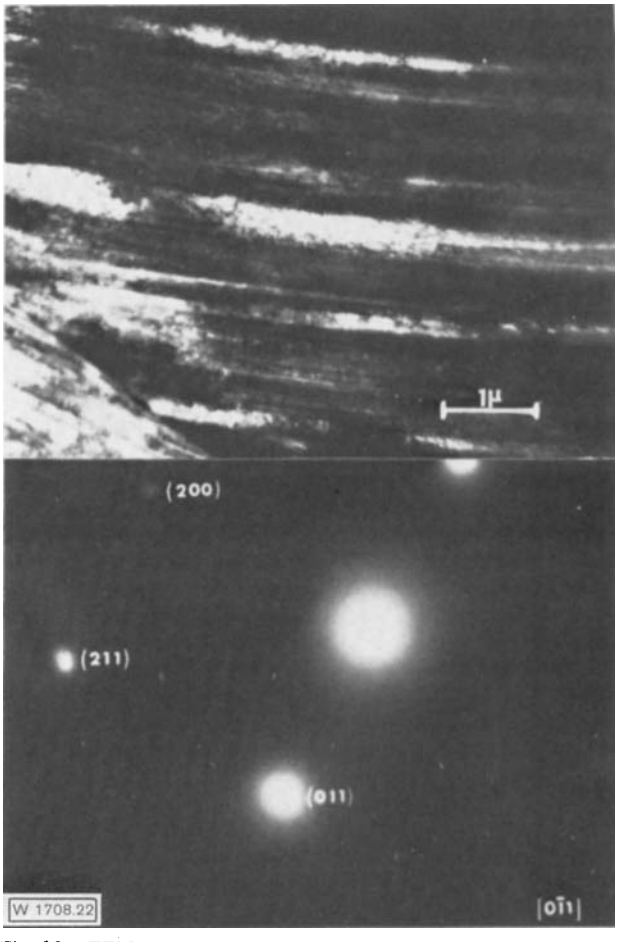

Fig. 22. TEM and selected-area electron diffraction pattern showing the identification of α'-cubic martensite in some deformation bands on AISI type 304 L steel deformed 30 per cent. T surface

The microstructural effect of varying the deformation degree between 0% and the maximum value has been analyzed in the case of the AISI 304 L: the density of the surface defects does not increase progressively with the deformation degree, for which, on the contrary, the existence of a critical threshold of influence of about 15% is found.

Finally, so far as concerns the effect of orientation of the surface examined with respect to the deformation direction, for the steel AISI 304 L work-hardened to the extent of 30% no significant difference was found between the three orientations T, L and 45 °l.

Discussion

As a whole, the results obtained on the electrochemical and corrosion behaviour of the austenitic stainless steels appear to confirm the hypothesis put forward previously (4), that the influence exerted on the resistance to generalized corrosion in the active region by the degree of cold plastic deformation of the material and by the orientation of the

*) In which the dislocations are concentrated in the boundaries of zones that are relatively free of them.

**) Magnetic measurements have given for the quantity (w/o) of α' martensite in AISI 304 L deformed 30 per cent, values within the range 2–4%.

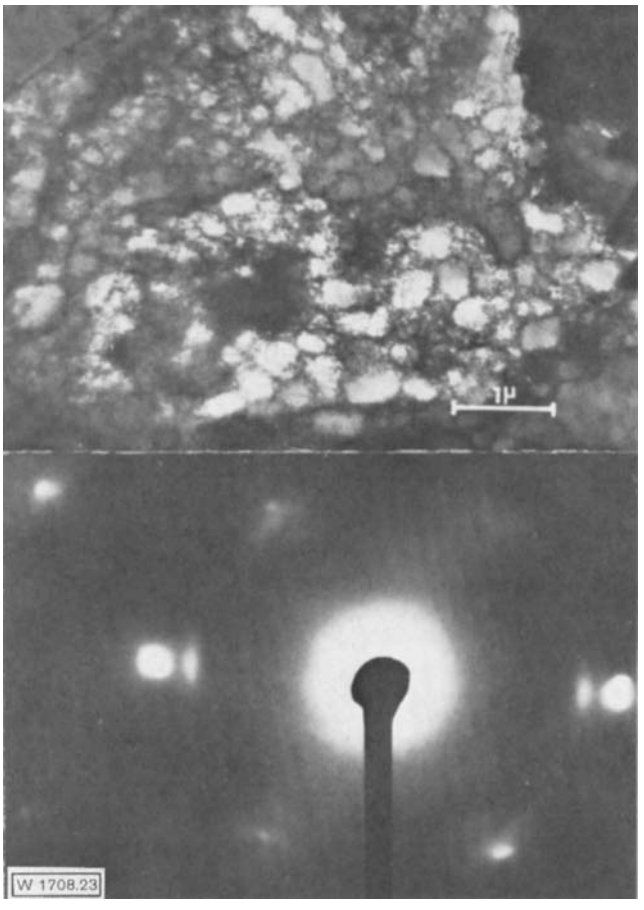

Fig. 23. TEM and selected-area electron diffraction pattern respectively showing the "cell structure" of the dislocations on nickel deformed 30 per cent and the disorientation among the cells. T surface

exposed surface with respect to the deformation direction is explained essentially by a decrease in the overvoltage of the cathodic hydrogen evolution, the anodic overvoltage of the dissolution of the metallic material remaining practically unchanged under our conditions with variation in the above-mentioned factors. The same considerations apply to the case of nickel, while for iron also an influence by way of the anodic process is certainly involved.

Passing now to a substantiation of this hypothesis in terms of the structure of the materials as shown by our investigation, it is useful in the first place to remember that a priori the "structural" effects induced by cold plastic deformation are dual: on the one hand, cold deformation produces preferred orientation of the crystal grains along the deformation direction with the appearance of a fibrous texture and consequent anisotropy in the overvoltages; on the other hand, it leads to an increase in the number of types, an alteration in the distribution, and an increase in the density of lattice defects emerging on the electrode surface. Hence the decreases in the hydrogen overvoltage that are found for the deformed material, in dependence on the deformation degree and the orientation of the electrode surface with respect to the deformation direction, could, a priori, be derived from both these structural effects.

As has been observed above, the cold plastic deformation of the materials by the application of a tensile stress has permitted the first effect, i. e. that of preferred orientation of the crystal grains, to be regarded as negligible. It is nevertheless significant in this connection to recall some of the previous results relating to the case of cold-drawing, in which the material undoubtedly assumed a certain degree of fibrous texture. As a matter of fact, X-ray investigations have indicated (4) for drawn steel AISI 304 L a certain alignment of the grains in the ⟨1 1 1⟩ direction, the direction to which the highest values of the hydrogen overvoltage correspond, according to measurements performed in this Institute on the various faces of single-crystals of austenitic stainless alloy (7). It may therefore be concluded that in any case the decrease in the hydrogen overvoltage observed on the deformed material (including material deformed by cold-drawing (4)) must be ascribed to the increase in structural defects emerging on the electrode surface.

We must now examine this correlation from a quantitative point of view and explain why anodic dissolution is not affected by the state of high surface defectiveness brought about by cold plastic deformation.

So far as concerns the first point, one may point out the agreement (shown in particular for AISI 304 L) in the value of the critical threshold of the influence of the degree of work-hardening both as regards the corrosion rate (or the hydrogen overvoltage) and the state of surface defectiveness, and also the discrepancy that exists between the sequence of increasing susceptibility of the various austenitic stainless steels to the effect of deformation with respect to the corrosion rate or the hydrogen overvoltage, i. e.

AISI 316 < AISI 304 < AISI 304 L

and, on the other hand, the sequence according to which, for the same deformed materials, the density of the deformation bands increases, i. e.

AISI 316 < AISI 304 L < AISI 304.

In our opinion, the inversion of the behaviour between AISI 304 and 304 L must be ascribed not so much to a quantitative question of densities of the deformation bands but to a qualitatively different effect induced by the deformation in the case of the AISI 304 L, i. e. to the phase transformation of austenite to martensite (which is also shown by our structural investigation). A confirmation and a more complete delimitation of the validity of this hypothesis could be derived from a broader study of the electrochemical behaviour (especially as concerns the hydrogen overvoltages) of austenitic stainless steels containing controlled and increasing quantities of martensite generated by tension at room temperature (8). At the present time, however, in this connection we may emphasize the importance of the influence exerted on the structural stability (or instability) of an austenitic stainless steel, and hence on the extent of the martensitic transformation (with equal rates of deformation and with the same nature of the deformation), by the composition of the steel itself, even within the range of a given type (8). Consequently, a considerable lack of reproducibility of the results for steels used technologically can be foreseen.

Going on to the other materials investigated, it may be observed how the absence of deformation bands found on the nickel even for high degrees of deformation (while the effect of the deformation is shown in the distribution of the dislocations, which are increased in number as well, according to a cell structure) does in fact correlate with the inconsiderable influence of the deformation degree on the corrosion rate.

In the case of iron, the decoration of the dislocations observed (for the present on non-work-hardened material) indicates an important role played in the activation of the cathodic process by possible precipitates (for example, cementite in a very finely divided form) or by interstitial atoms (for example, carbon and/or nitrogen atoms) locali-

zed in correspondence with the dislocations*). The literature contains extensive documentation on the decrease in the hydrogen overvoltage on passing from iron to cementite (9), or from highest-purity iron (zone-refined, C < 0.001%) to iron in which 0.025% of carbon is present**) (10).

Discussing the more strictly structural aspects, it can be seen that the results of the comparative electron microscope examination of the nature, density, and distribution of the lattice defects for the various materials considered both in the "as received" state***), and in the deformed state****) are not only in accord with the values reported in the literature for stacking fault energies (some 20 ergs/cm^2 for an 18–8 stainless steel and 150–300 ergs/cm^2 for nickel, both with an fcc lattice, while for iron, with a bcc lattice, this energy is still higher (11) but they also indicate, within the three types of austenitic stainless steel, an increase in the stacking fault energy in the sequence:

AISI 304 < AISI 304 L < AISI 316×).

As a matter of fact, in the case of low stacking fault energies cold plastic deformation leads to the appearance of bands corresponding, for example, to a concentration of dislocations in the slip planes or to deformation twins formed through a sequence of stacking faults in successive planes and therefore associated with restricted slip, while when the stacking fault energy is high one arrives at a cell structure through cross slip processes of the screw dislocations (and perhaps also climb processes of the edge dislocations) (12).

The described situation is also in harmony with the correlation proposed by various authors (13) between the stacking fault energy and the presence of restricted slip or cross slip and the susceptibility to stress corrosion of metallic materials with an fcc lattice, in the sense that those materials characterized by a high density of stacking faults, i. e. with a correspondingly low stacking fault energy and therefore with restricted slip, are subjected to this form of corrosion.

Passing now to the correlation between the structural effects of cold plastic deformation and anodic behaviour in the active region, the results obtained enable us to state that, for the materials considered××), any influence of even a high degree of surface defectiveness is substantially masked by their electrochemical "inertia". In other words in the "inert" metals according to *Piontelli's* classification (14) the structural factors on atomic and molecular scale, and therefore the nature of the bonds which, on the basis of the particular electronic configuration of these metals (incomplete electron subshells) bind the ions to be exchanged with the solution, appear to overcome the structural factors on the lattice scale, i. e. the nature, distribution, and density of the lattice defects emerging on the electrode surface and the crystallographic orientation. It is appropriate to mention in this connection how the extensive research work performed at this Institute on the electrochemical behaviour of metal single-crystals with oriented surface (15) shows that, in the case of the "inert" metals, the influence of crystallographic orientation on the ion-exchange overvoltage is slight or negligible, while on the corresponding hydrogen overvoltages it is higher. It therefore seems possible to conclude that an influence of the structural factors on the lattice scale mentioned above can be shown only on the process of hydrogen evolution, for which the "inert" metals, because of their very nature, already appear as "activators"+).

What has been said with reference to pure metals may be regarded as also referring to the alloys that we have considered, as is confirmed by the very small variations in the lattice parameters on passing from the former to the latter++), or even directly be the values of the kinetic electrochemical parameters given in the literature+++).

The conclusions drawn concerning the correlation between structural effects of cold plastic deformation and anodic behaviour in the active region obviously relate to our working conditions in which the samples were **first** deformed and subsequently subjected to the electrochemical measurements, during the performance of which the state of surface defectiveness could therefore remain constant. In contrast, the conditions in which the deformation is applied with a constant rate of increase up to the fracture of the test-piece si**multaneously** with the performance of the electrochemical measurements++++) (conditions under which the dislocations multiply and move during the measurements until they appear on the anode surface, with a consequent continuous increase in the state of defectiveness of the surface) are radically different. Nevertheless, it seems to us that, taken as a whole, the results of our electrochemical measurements and microstructural investigations can support those authors who advocate a reconsideration of the role of hydrogen evolution in stress corrosion cracking even in the case of some austenitic stainless steels (18).

The influence of the degree of work-hardening on the anodic behaviour of the materials considered outside the ac-

*) See Foroulis in ref. (1).

**) See the footnote +++) on this page

***) Stacking faults, which decrease in density from AISI 304 to 304 L; absence of this type of defect in steel AISI 316, nickel and iron, absence to which a tendency of the dislocations to become grouped into cells is opposed in the case of the nickel.

****) Deformation bands also consisting of deformation twins, the density of which decreases from AISI 304 to 304 L and 316, with corresponding superposition of a cell structure, which is the only one that exists in the case of nickel.

×) This increase can be related to the rise in the nickel content on passing from steel AISI 304 to 304 L and 316 (see Table 2 and *Swann* in ref. (13), in spite of the decrease in the stacking fault energy caused by the molibdenum addition in steel AISI 316 (see the first and second paper in ref. (13)).

××) With the exception of iron, in which case the difficulties of examination in an electron-microscope for the present preclude any attempt at explaining on a microstructural basis the decrease in the anodic overvoltage observed at higher degrees of work-hardening.

+) Apart from the possible causes of heterogeneity brought into play by the process of deformation, such as precipitation of new phases, phase transformations, segregation of impurities, local variations in surface chemical composition due to the appearance of segregates on the surface, etc., with the possible formation of more active anodic areas.

++) For example, for the alloy with the composition Fe 71%, Cr 15%, Ni 14%, C ~ 100 ppm, single-crystals of which (fcc) have been prepared in this Institute, we have a = 3.57 Å (16), as compared with a = 3.564 Å for γ-Fe.

+++) For example, *Greene* and *Saltzman* (1) report the following values of exchange current density at 25 °C for a carbon steel (C 0.08%):

$i_{oFe} = 0.0015\ \mu A/cm^2$, $i_{oH_2} = 0.43\ \mu A/cm^2$.

According to the results of *Bockris* and *Drazic* (10), on passing from zone-refined iron (C < 0.001%, total impurities < 0.01%), to iron containing 0.025% of C (total impurities 0.2%) the metal ion-exchange current density at 25 °C remains practically unchanged: $i_{oFe} \sim 0.02\ \mu A/cm^2$, while for the hydrogen evolution process there is an increase in i_{oH_2} from 0.8 to 8 $\mu A/cm^2$.

For the above-mentioned alloy with the composition Fe 71%, Cr 15%, Ni 14%, C ~ 100 ppm, *Peraldo Bicelli* and *Romagnani* (17) report the values $i_{oH_2} = 0.87–4.2\ \mu A/cm^2$.

++++) See, for example, the investigations of *Hoar* and his co-workers and of other authors cited in (2) on the so-called "mechano-electrochemical effect"; see also *Hoar* in (13).

tive region is in agreement with the results of other authors*).

In the case of iron the influence of the position of the electrode surface in the solution and the particular shape of the anodic polarization curves beyond the active region, suggest the presence of an initial "sulphation" process which involves formation of a supersaturated solution leading to crystallization of ferrous sulphates**) in form of a porous layer (20), with subsequent true passivation at more noble values of the electrode potential***), owing to formation of more protective films of oxides or hydroxides of the metallic form of higher valence. The difference in shape +) between the two curves relating to the two positions of the electrode surface (horizontal facing upwards and vertical) is then due to stratification of the corrosion products on the electrode, which is easier in the first position, with a consequent more effective initial covering.

On the other hand, in the case of nickel the shape of the polarization curves with the appearance of a pseudo-passivation peak, according to several other authors (21) suggests the presence of a first stage of pseudo-passivation, owing to electrochemical formation of a porous non-protective film of NiO, followed by a stage of true passivation at more noble values of the electrode potential, owing to formation of protective films of oxides of the metallic forms of higher valence. Contrary to all expectation, the passivating films formed on work-hardened material (at higher potential values and therefore with greater difficulty, especially for the L surfaces) are more protective than the ones formed on "as received" material, as indicated by the passive currents which are smaller in the former case, in spite of larger width of the passive region in the latter.

A final point to be discussed relates to the effect of variations in surface chemical composition on the course of the corrosion phenomena of the materials studied before the achievement of steady conditions, effect that can already be deduced from the decrease in time shown by the corrosion rate in the active region in the case of nickel and AISI 304 and 304 L, but which is shown most strikingly in the anomalous curves of the corrosion rate vs. time in the case of the AISI 316 (T and 45 °I surfaces).

In our opinion the principle of the surface enrichment in the most noble element, which is at the basis of the theory of the anodic dissolution of homogeneous alloys (22), must be connected (and this also for understanding the behaviour of the AISI 316) with the consideration that even in the initial condition it is possible that the surface concentrations of alloy elements present in small amounts or of impurities are greatly superior to the corresponding bulk concentrations following the thermal or mechanical treatments that the material has undergone. For example, for an AISI 316 rolled into sheets with a thickness of 1.25 mm a surface concentration of molybdenum of the order of 14%, as compared with a bulk value of 1.95%, has been found by *Auger* electron spectroscopy (23)×). The play in the changes of surface chemical composition during the anodic dissolution of AISI 316 (deformed cold and/or hot), which is capable of observable effect on the electrochemical behaviour of the steel and, in addition, is dependent on the deformation degree and the orientation of the exposed relative to the deformation direction, may therefore also be due to a considerable extent to such an element, (i. e. molybdenum), besides, of course, to chromium, nickel and iron.

It is obvious that only further direct and indirect observations can contribute to the elucidation of these last points.

*) See *France* in (1) for rimmed steel AISI type 1008 and *Di Bari* and *Petrocelli* (19) for nickel.

**) Crystallization which, in the case of the iron work-hardened to the maximum extent, begins at slightly less noble potentials because of the lower value of the anodic overvoltage.

***) In the range from -100 to 0 mV vs. SSE.

+) Before the range of potentials mentioned above (-100 to 0 mV vs. SSE).

×) Similarly, for an AISI 304 containing 0.45% of molybdenum the surface concentration was found to be 3%.

(Eingegangen: 16. 11. 1973)

References

1. *G. Tammann, F. Neubert:* Z. anorg. allg. Chemie **207**, 87 (1932). *O. Bauer, O. Kröhnke, G. Masing:* Die Korrosion metallischer Werkstoffe, Band I, Hirzel, Leipzig 1936, p. 314; see also Corrosion Handbook, *H. H. Uhlig* Ed., Wiley, New York 1948, p. 138. *C. A. Edwards, D. L. Phillips, D. F. G. Thomas:* J. Iron Steel Inst. **137**, 223 (1938); see also Corrosion Handbook, *H. H. Uhlig* Ed., Wiley, New York 1948, p. 576. *M. T. Simnad, U. R. Evans:* Trans. Faraday Soc. **46**, 175 (1950). *N. D. Greene, G. A. Saltzman:* Corrosion **20**, 293 t (1964). *Z. A. Foroulis, H. H. Uhlig:* J. Electrochem. Soc. **111**, 522 (1964). *Z. A. Foroulis:* Corrosion Sci. **5**, 39 (1965). *F. Zucchi, G. L. Zucchini, G. Trabanelli, L. Baldi:* Electrochim. Metall. **1**, 400 (1966). *W. D. France Jr.:* Corrosion **26**, 189 (1970). *R. Franks:* in: Corrosion Handbook, *H. H. Uhlig* Ed., Wiley, New York 1948, p. 159. *H. R. Copson:* in: Corrosion Handbook, *H. H. Uhlig* Ed., Wiley, New York 1948, p. 576. *G. Trabanelli, F. Zucchi:* Electrochim. Metall. **1**, 251 (1966).
2. *T. P. Hoar:* in: Modern Aspects of Electrochemistry, Vol. 2, *J. O'M. Bockris* Ed., Butterworths, London 1959, p. 334; *T. P. Hoar, J. M. West:* Nature **181**, 835 (1958); *T. P. Hoar, J. C. Scully:* J. Electrochem. Soc. **111**, 348 (1964); *A. Windfeldt:* Electrochim. Acta **9**, 1139 (1964); *A. R. Despic, R. G. Raicheff, J. O 'M. Bockris:* J. Chem. Phys. **49**, 926 (1968); *R. P. Frankenthal:* Corrosion Sci. **8**, 491 (1968); *M. Pražák, M. Havrda:* Proceedings 4th Int. Congress on Metallic Corrosion, Amsterdam 1969, NACE, Houston 1972, p. 130.
3. *J. J. Harwood:* Corrosion **6**, 249 (1950); *U. R. Evans:* Corrosion and Oxidation of Metals, Arnold, London 1960, p. 386 and 388.
4. *W. Nicodemi, P. Pedeferri, D. Sinigaglia:* La Metall. Italiana **63**, 23 (1971); *D. Sinigaglia, P. Pedeferri, B. Mazza, G. Galliani, L. Lazzari:* La Metall. Italiana **65**, 77 (1973).
5. *P. Coulomb:* Les textures dans les métaux de réseau cubique Dunod, Paris 1972, p. 93.
6. *M. Stern, A. L. Geary:* J. Electrochem. Soc. **104**, 56 (1957).
7. *A. La Vecchia, L. Peraldo Bicelli, C. Romagnani:* Ann. Chimica **62**, 489 (1972); see also *N. D. Greene, G. A. Saltzman* in ref. (1).
8. *D. Rousseau, G. Blanc, R. Tricot, A. Gueussier:* Mém. Sci. Rev. Metallurg. **67**, 315 (1970).
9. *D. N. Staicopolus:* J. Electrochem. Soc. **110**, 1121 (1963).
10. *J. O 'M. Bockris, D. Drazic:* Electrochim. Acta **7**, 293 (1962).
11. *J. Bénard, A. Michel, J. Philibert, J. Talbot:* Métallurgie générale, Masson, Paris 1969, p. 154. See also ref. (5), p. 74.
12. *P. B. Hirsch:* J. Inst. Metals **87**, 406 (1958/9).
13. *R. Stickler, S. Barnartt:* J. Electrochem. Soc. **109**, 343 (1962); *S. Barnartt, R. Stickler, D. van Rooyen:* Corrosion Sci. **3**, 9 (1963); *P. R. Swann:* Corrosion **19**, 102 t (1963); *M. Watanabe, Y. Mukai:* Proceedings 4th Int. Congress on Metallic Corrosion, Amsterdam 1969, NACE, Houston 1972, p. 83; see also *T. P. Hoar, J. C. Scully* in ref. (2); for an extensive review see *T. P. Hoar:* Corrosion **19**, 331 t (1963).
14. *R. Piontelli:* Elementi di teoria della corrosione a umido dei materiali metallici, Longanesi, Milano 1961, p. 166 and 288.
15. *R. Piontelli:* Electrochim. Metall. **1**, 5 (1966); *R. Piontelli, G. Poli, G. Serravalle:* in: *Yeager:* Transactions of the Symposium on Electrode Processes, Wiley, New York 1961, p. 67; *R. Piontelli, M. Lazzari, B. Rivolta:* Ist. Lomb. (Rend. Sci.) A **99**, 277 (1965); *R. Piontelli, L. Peraldo Bicelli, A. La Vecchia:* Rend. Acc. Naz. Lincei VIII, **27**, 312 (1959); *R. Piontelli, L. Peraldo Bicelli, C. Romagnani:* Rend. Acc. Naz. Lincei VIII, **34**, 233 (1963); *R. Piontelli, B. Rivolta, B. Mazza, F. Magnoni:* Ist. Lomb. (Rend. Sci.) A **97**, 282 (1963); *R. Piontelli, B. Rivolta,*

M. Lazzari, A. La Vecchia: Ist. Lomb. (Rend. Sci.) A **98**, 372 (1964); *R. Piontelli, B. Rivolta, M. Lazzari, A. La Vecchia:* Ist. Lomb. (Rend. Sci.) A **98** 387 (1964); *R. Piontelli, L. Peraldo Bicelli, M. R. Graziano, A. La Vecchia:* Rend. Acc. Naz. Lincei VIII, **32**, 445 (1962); *R. Piontelli, L. Peraldo Bicelli, A. La Vecchia:* Rend. Acc. Naz. Lincei VIII, **32**, 827 (1962); *R. Piontelli, L. Peraldo Bicelli, A. La Vecchia:* Cobalt **18** (March 1963); *R. Piontelli, L. Peraldo Bicelli, C. Romagnani:* Rend. Acc. Naz. Lincei VIII, **34**, 480 (1963); see also *A. La Vecchia, L. Peraldo Bicelli, C. Romagnani* in ref. (7).

16. *M. Lazzari, B. Rivolta:* Ann. Chimica **61**, 227 (1971).
17. *L. Peraldo Bicelli, C. Romagnani:* Chim. Ind. (Milano) **53**, 1128 (1971).
18. *P. R. Rhodes:* Corrosion **25**, 462 (1969); *R. J. Asaro, A. J. West, W. A. Tiller:* paper presented at the "International Conference on Stress Corrosion Cracking and Hydrogen Embrittlement of Fe-Cr-Ni-Base Alloys", Unieux – Firminy, France, 1973; *N. A. Nielsen:* Ibid.; for a review see: *G. J. Theus, R. W. Staehle:* Ibid.; *R. W. Staehle:* in: The Theory of Stress Corrosion Cracking in Alloys, *J. C. Scully* Ed.; NATO, Brussels 1971, p. 223.
19. *G. A. Di Bari, J. V. Petrocelli:* J. Electrochem. Soc. **112**, 99 (1965).
20. *T. P. Hoar:* in: Modern Aspects of Electrochemistry, Vol. 2, *J. O'M. Bockris* Ed., Butterworths, London 1959, p. 287, 288; *U. R. Evans:* Corrosion and Oxidation of Metals, Arnold, London 1960, p. 231, 232; *J. G. Hines, R. C. Williamson:* Corrosion Sci. **4**, 201 (1964); *R. C. Williamson, J. G. Hines:* Corrosion Sci. **4**, 221 (1964); *G. Gilli, F. Zucchi:* Corrosion Sci. **8**, 801 (1968).
21. *N. D. Greene:* First International Congress on Metallic Corrosion, Butterworths, London 1962, p. 113; *E. Kunze, K. Schwabe,* Corrosion Sci. **4**, 109 (1964); *R. R. Sayano, K. Nobe:* Corrosion **22**, 81 (1966); *T. S. De Gromoboy, L. L. Shreir:* Electrochim. Acta **11**, 895 (1966); *N. Ya. Bune:* Protection of Metals **3**, 36 (1967); *F. Zucchi, G. Trabanelli:* Electrochim. Metall. **4**, 313 (1969); *G. Gilli, P. Borea, F. Zucchi, G. Trabanelli:* Corrosion Sci. **9**, 673 (1969).
22. *R. F. Steigerwald, N. D. Greene:* J. Electrochem. Soc. **109**, 1026 (1962).
23. *G. J. Barnes, A. W. Aldag, R. C. Jerner:* J. Electrochem. Soc. **119**, 684 (1972).

Anodische Polarisationskurven von Messinglegierungen in Ammoniumchloridlösungen

Von *R. Bartoníček*

G. V. Akimov, Staatliches Forschungsinstitut für Materialschutz, Prag

Die anodische Auflösung von Messinglegierungen ist bereits mehrfach untersucht worden (1–8). Das Verhalten einer Legierung ist abhängig von ihrer Zusammensetzung, wobei sich kupferreiche Legierung ähnlich wie Kupfer verhalten. In Chloridlösungen, in denen eine Schicht festen Kupferchlorids entsteht, verschiebt sich das Potential des Beginns der anodischen Auflösung der Legierung mit deren abnehmendem Kupfergehalt zu negativen Werten. Aber das Potential der Passivierung erhöht sich, und gleichzeitig damit nimmt auch der für die Passivierung erforderliche Strom zu (2, 4). Die Beziehung zwischen diesen Werten und der Zusammensetzung der Legierung und ihrer Struktur ist jedoch bis jetzt noch nicht geklärt worden.

Experimenteller Teil

Für die Messungen wurden Proben gegossener Messinglegierungen verwendet, die aus Elektrolytkupfer und Zink (Eisengehalt unter 0,01%, Manganspuren) hergestellt worden waren. Die gegossenen Proben wurden wärmebehandelt, dann in Gießharz eingebettet, so daß Elektroden mit einer Oberfläche von 0,3 cm^2 erhalten wurden. Angaben über Kupfergehalt, Wärmebehandlung und Struktur der Proben zeigt die nachstehende Tabelle.

Bezeichnung	Kupfergehalt %	Wärmebehandlung	Struktur
1	2	3	4
Cu	99,99		rekristallisierte Struktur
Cu87Zn13	87,1	800 °C, 1 h/	α
Cu79Zn21	79,4	luft-	α
Cu69Zn31	69,4	gekühlt	α
Cu62Zn38	62,1		α geringe Menge β
Cu54Zn46	53,9		β
Cu49Zn51	49,4		β mit fein ausgeschiedener γ-Phase in Körnern
Cu40Zn60	40,5	700 °C, 1 h/	γ
Cu30Zn70	30,4	luft- gekühlt	γ und darin abgeschiedene ϵ-Phase
Cu26Zn74	26,4		γ und darin eine größere Menge ϵ-Phase abgeschieden
Cu8Zn92	8,3	350 °C 1 h/luft- gekühlt	ϵ und darin dendritisch abgeschiedene η-Phase
Zn	99,9		rekristallisierte Struktur

Alle Proben hatten grobes Korn. Ihre Oberfläche wurde mit feinem Korund (Körnung 600) geschliffen, in Benzol und Äthanol gereinigt und nach Verdunsten der Lösungsmittel in den mit Argon gesättigten Elektrolyten getaucht.

Der Elektrolyt wurde aus zweifach destilliertem Wasser und chemisch reinen Chemikalien hergestellt. Die Prüflösung wurde auf 25 °C ± 0,1 °C gehalten und hatte zur vertikal angebrachten Kupferfläche freien Zutritt.

Die potentiodynamische Polarisation wurde mit einem elektronischen Potentiostaten Type SVUOM Ple-05*) mit Sägezahngenerator Type SVÚOM G-01 vorgenommen, bei dem die Geschwindigkeit des linearen Anstiegs der Polarisationsspannung eingestellt werden konnte und eine reversible Polarisation bei jedem beliebigen Potential möglich ist. Das Potential wurde gegen eine gesättigte Kalomelelektrode gemessen, die mit der Lösung durch eine mit gesättigter Kaliumchloridlösung gefüllte elektrodische Brücke verbunden war. Im Text und auf den Abbildungen sind die Potentiale in der Wasserstoffskala angeführt. Der Strom wurde mit einem Milliamperemeter (Type Vareg) gemessen. Aufgezeich-

*) SVÚOM – Staatl. Forschungsinstitut für Materialschutz.